Inhibition of Sulfate-reducing Bacteria Presence in Masonry via High-Performance Sol-Gel Coatings

F. Akande[1,2], P. P. Rojaz[1,3], N. Salinas[1,5], C. Taylor[1], J. Bao[6], C. Qin[6], S. A. Curran [1,4]

[1] Curran Nanotechnology Research Group (CNRG), University of Houston, Houston, TX 77204, USA
[2] College of Education, University of Houston, Houston TX 77204, USA
[3] Department of Chemical Engineering, University of Houston, Houston TX 77204, USA
[4] Department of Physics, University of Houston, Houston, TX 77204, USA
[5] College of Natural Sciences and Mathematics, Science and Research Building 2, 3455 Cullen Blvd #342, University of Houston, Houston TX 77204, USA
[6] Department of Electrical and Computer Engineering, University of Houston, Houston TX 77204, USA

Abstract

Microbially Influenced Corrosion (MIC) of concrete infrastructure accounts for a significant portion of the $2.5 trillion annual global cost of metal and concrete degradation. Existing MIC mitigation relies on epoxy barriers or antimicrobial admixtures that often fail due to poor interfacial bonding or pose a significant environmental risk. This study evaluates a novel hybrid organic-inorganic sol-gel coating designed to create a chemically integrated, antimicrobial shield. Comparative testing was deployed to examine the antimicrobial performance of Sol-158-3. While each test demonstrated a significant bacterial presence, Sol-158-3 maintained a stable, low-microbial profile throughout testing. This presents a proactive strategy for mitigating microbial in masonry, effectively eliminating MIC. Notably, the pure sol-gel outperformed a sample modified with the biocide IPBC, suggesting that the structural density of Sol-185-3's network is more critical for MIC resistance than secondary organic additives. By inhibiting early-stage neutrophilic colonization and maintaining surface alkalinity, this sol-gel intervention effectively disrupts the biogenic sulfur cycle. These findings provide a sustainable, cost-effective pathway for extending the service life of critical masonry infrastructure.

Introduction

Corrosion in concrete refers to the chemical degradation of the material caused by reactions with its surrounding environment. Recognized as a major durability issue, corrosion is a global crisis that contributes an estimated $2.5 trillion annually in repair and maintenance [1]. In the United States alone, annual costs reach approximately $276 billion, a substantial portion of which stems from the degradation of concrete structures protecting steel infrastructure, such as pipelines [2,3,4]. Despite concrete's versatility and strength, its vulnerability in sewer systems, marine environments, and oil pipelines poses severe safety risks and reduced structural integrity. While purely chemical corrosion is the traditional focus, recent research highlights the critical role of biogenic deterioration, widely known as microbially influenced corrosion (MIC) [5].

Portland cement is a powdery substance made up of calcium silicates and aluminate mineral phases, such as belite ($2CaO \cdot SiO_2$), alite ($3CaO \cdot SiO_2$), tricalcium aluminate ($3CaO \cdot Al_2O_3$) and brownmillerite ($4CaO \cdot Al_2O_3 \cdot Fe_2O_3$) [6]. When mixed with water, the compounds in Portland cement hydrate to form the 'glue' that binds all the aggregates together in concrete, mortar, grouts, and stuccos. Due to the high alkalinity of calcium phases, the hydrated cement is inherently vulnerable to neutralization reactions when exposed to aggressive acids like hydrochloric acid (HCl), atmospheric nitric acid (HNO_3), and biogenic sulfuric acid (H_2SO_4) produced by microbial activity [7]. Acidic attacks such as these chemically dissolve the binders present in concrete, destroying the structural cohesion of the aggregate composition, which causes the concrete to crumble, ultimately leading to severe degradation of cement-supported infrastructure.

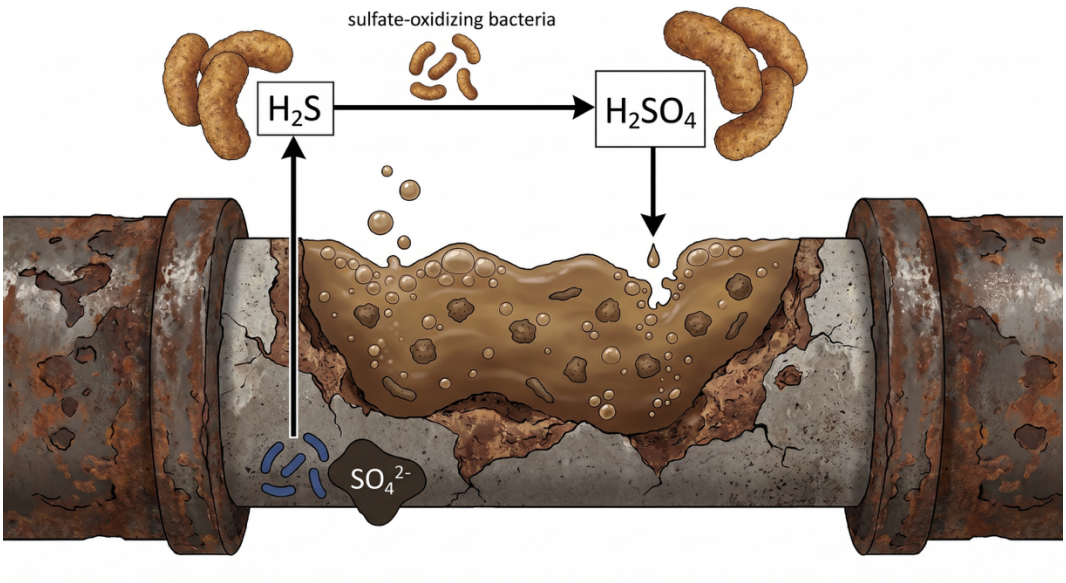

Figure 1. *The biogenic sulfur cycle that leads to microbially influenced corrosion in concrete or sewer pipes or concrete cladding used around steel pipes used in oil and fracking operations.*

Corrosion of reinforced concrete proceeds through biogenic processes. Sulfate-reducing bacteria (SRB) from the genus *Desulfovibrio* are the primary agents for biogenic deterioration because of their role in MIC, contributing to more than half of MIC incidents. In fracking sites, corrosion tests and gene sequencing have identified corrosive strains from the *Desulfomicrobiaceae* and *Desulfovibrionaceae* families across injection water and both low- and high-viscosity fracking water, causes softening, spalling, and structural damage. These strains function as the primary drivers of sulfate reduction within hydraulic fracking fluid, causing the degradation of pipe-enshrouded and open frack sites. These microbes not only survive but also thrive in the high-salinity and high-pressure, oxygen-poor environments of oil and gas wells or well baths made of concrete. As chemo-organotrophic organisms, *Desulfovibrio spp.* commonly use simple organic compounds, like lactate and pyruvate produced by neighboring bacteria, as electron donors [8]. Furthermore, *Desulfovibrio* can utilize hydrogen and acetate to reduce sulfate ions, a process facilitated by the crucial enzymes hydrogenase and cytochrome C, which manage the electron transport system necessary for sulfate reduction [9,10].

Sewer systems and deeply embedded pipelines often exist in oxygen-low environments where SRB thrive. Additionally, the deep pores of masonry contribute to an anaerobic environment; as water enters pores found in masonry, oxygen is dispelled [11]. Sulfate-rich water penetrates masonry through capillary action, creating the favorable anaerobic environment SRB requires. As shown in Eq. 1, SRB biofilms consume sulfates that naturally occur in wastewater, producing hydrogen sulfide (H_2S) [12]. Once produced, H_2S can react with calcium hydroxide ($Ca(OH)_2$), naturally found in concrete mixes [13]. This reaction, occurring alongside abiotic carbonation (the interaction with atmospheric CO_2), leads to the formation of thiosulfates (CaS_2O_3) and polythionic acids, as demonstrated in Eq. 2. The formation of these intermediates depletes the available calcium hydroxide ($Ca(OH)_2$), effectively lowering the pH of the environment from around 13 to 9, creating a suitable environment for the initial colonization of neutrophilic sulfate-oxidizing bacteria to oxidize H_2S into sulfuric acid (H_2SO_4), a highly corrosive agent [14].

$$SO_4^{2-} + 2C_{org} + H_2O \rightarrow 2HCO^{3-} + H_2S \qquad (1)$$

$$2H_2S + 2O_2 + Ca(OH)_2 \rightarrow CaS_2O_3 + 3H_2O \qquad (2)$$

Alternatively, unreacted H2S gas can diffuse outwards towards the oxygen-rich surface of masonry. There, neutrophilic bacteria oxidize rising H2S into elemental sulfur (S0) using the available atmospheric oxygen. As shown in Eq. 3, this produced sulfur serves as the substrate for more aggressive, acidophilic bacteria to further oxidize H_2S into the highly corrosive H_2SO_4 [15-18]. The produced sulfuric acid aggressively attacks surrounding calcium hydroxide to form gypsum ($CaSO_4 \cdot 2H_2O$) and ettringite ($CaO \cdot Al_2O_3 \cdot 3CaSO_4 \cdot 32H_2O$). While gypsum is a solid, it's structurally weak and easily washes away, leaving the concrete porous and resulting in the loss of aggregates [19].

$$H_2S + 2O_2 \rightarrow H_2SO_4 \qquad (3)$$

Onshore rigs operate in fracking basins in areas such as the Permian, Marcellus, Eagle Ford, and more [20]. Water-based drilling fluids (muds) are the dominant type used by the rigs in U.S. fracking operations. Recent scholarly reviews confirm that water-based muds (WBM) hold the majority of market share onshore due to lower cost, environmental regulations, and performance improvements. Oil-based muds (OBM) are used occasionally but are not the norm [21]. Unlike OBMs, WBMs contain high volumes of water and biodegradable additives that act as food sources for present bacterial strains. The depths of the cement jacket in hydraulic fracturing wells, based on DOE/NETL-supported studies, vary by casing string. Surface casing, along with cement sheath, is typically set from the surface to depths ranging from several hundred to more than 2,000 feet below the surface. The depth is required to extend below usable drinking water aquifers with cement pumped to the surface to ensure complete zonal isolation [22]. At U.S. shale sites, the average vertical depth to the target oil is approximately 8,300 feet, with horizontal lateral extending an additional 5,000-10,000 feet. Therefore, the full cement jacket protects the casing across thousands of feet [23]. While cement jacket protection is innately effective, a single failure caused by biogenic processes, like the production of sulfuric acid by bacteria within the WBM, can lead to massive environmental and financial costs. A report on casing damages notes that roughly 7% of global oil wells experience casing failures, with some older fields reaching failure rates of up to 28.5% [24].

Current MIC mitigation strategies often target the internal steel while leaving the surrounding masonry vulnerable. Existing external barriers, such as epoxy coatings, are widely utilized for their initial strength, but are susceptible to micro-cracking and delamination under environmental stress, which allows aggressive substrates to bypass the protective barrier [25,26].

Nanocomposite modifications have attempted to correct this, but they frequently suffer from nanoparticle agglomeration, which results in a weakened, less effective barrier [27,28]. Alternatively, organic antimicrobial admixtures have been used to mitigate MIC. A common organic admixture, Iodopropynyl butylcarbamate (IPBC), is commonly used to mitigate MIC [29]. However, organic admixtures often fail to provide long-term protection and cannot withstand harsh, acidic environments, rendering them ineffective in treating MIC. Furthermore, the use of organic agents may potentially lead to microbial resistance against organic biocides. Similarly, inorganic antimicrobial agents utilize heavy metals or metal ions to inhibit bacterial enzymatic function. However, these nano-oxides used in inorganic antimicrobial agents are known to be environmentally toxic [30-32]. To address these limitations, this study evaluates a hybrid organic-inorganic sol-gel coating. Unlike traditional physical barriers, this sol-gel creates a chemically bonded, hydrophobic, and nanoporous network that integrates into the masonry surface. By restricting the capillary entry of sulfate-rich water, the coating effectively strips SRB of the nutrients required for growth. Through mass retention analysis, qualitative evaluation of bacterial growth, and FTIR spectra analysis, this study investigates the antimicrobial efficacy of this novel sol-gel under varying environmental conditions to demonstrate its potential for long-term, sustainable MIC mitigation.

Methods and Materials

Mass Retention under Acid Exposure:

Concrete block was treated with Sol-158-3 Masonry Sealer by foam roller and dried/cured. Pristine and Sol-158-3 Masonry treated concrete samples are dipped into 1M HCl or HNO_3 (both pH = 0). The concentration of acids used here is 100 to 10,000 times stronger than the acidity of a normal acid rain (pH 2-4).

Every 24 hours, both samples were retrieved from the acids and washed under running water, the concrete surface was hand-brushed slightly to remove any loose debris before weighing. Acids erode concrete by diffusion through water channels into cement particles and subsequently dissolve them. Sol-158-3 Masonry is a proprietary penetrating sealer that functions by rapidly permeating into the interior structure of the concrete and establishing a robust interpenetrating network, effectively sealing the cement structure of the concrete from the inside out. Sol-158-3 Masonry Sealer's innovative barrier encapsulates the cavities and pore spaces at the microscopic level within the concrete. Our desire at all times is to minimize the incursion of water which is caused by the erosion of masonry. Critically, the deeper wells go the more likely it is for fracturing, therefore, having an established presence of hydrophobicity is essential to operations. Sol-158-3 Masonry Sealer preemptively eliminates sources of water absorbed into concrete as well as the acids that water carries.

Qualitative Evaluation of Bacterial Growth:

Sol-158-3 was applied to the masonry samples via volumetric drop-casting using a micropipette to ensure a consistent application. A 0.1M HCl catalyst was utilized to drive polycondensation of the sol-gel network. During application, the alcohol-based solvent, methanol, facilitates miscible displacement of the residual pore water within the masonry samples. This interaction accelerated the drying phase as the alcohol-water mixture evaporates more rapidly than pure water. Furthermore, catalytic action ensures a rapid, uniform setting process, resulting in a higher quality, more cohesive protective jacket compared to traditional sealants.

The sulfate-reducing bacteria test was performed in four different environments:

Sample 0: The concrete sample was placed on a culture medium tailored to support the growth of such bacteria. The sample was placed in incubation at 30∘C for three days.

Sample A: The concrete sample was soaked in Sol-158-3 for two minutes and set to dry for another 15 minutes. The sample was placed in incubation at 30∘C for three days.

Sample B: The concrete sample was soaked in a solution of Sol-158-3/IPBC 10:2 for two minutes and set to dry for another 15 minutes. The sample was placed in incubation at 30∘C for three days.

Sample C: The concrete sample was soaked in a solution of Sol-158-3/IPBC 10:2 for two minutes, then re-coated with IPBC and set to dry for another 15 minutes. The sample was placed in incubation at 30∘C for three days.

Figure 2. *Photos of treated concrete samples after a 3-day incubation in a culture media designed to support bacterial growth.*

FTIR Spectroscopic Analysis

Fourier transform-infrared (FTIR) spectra were obtained using a Bruker Optics ALPHA-FTIR spectrophotometer in attenuated total reflection (ATR) mode outfitted with a ZnSe internal reflection element at 128 scans to average and a resolution of 2 cm-1 [33].

Results

Mass Retention under Acid Exposure

To evaluate the structural durability of the Sol-158-3, an acid erosion test was conducted in hydrochloric acid (HCl) over a multi-day period. As shown in Fig. 2, visual degradation and structural integrity changes were documented chronologically using time-lapse photography. The concrete block treated with Pristine (right) experienced rapid surface degradation, aggregate exposure, and significant structural crumbling within the submerged area. Conversely, the concrete block treated with Sol-158-3 (left) maintained its original shape and surface profile, exhibiting strong physical resistance to acid breakdown.

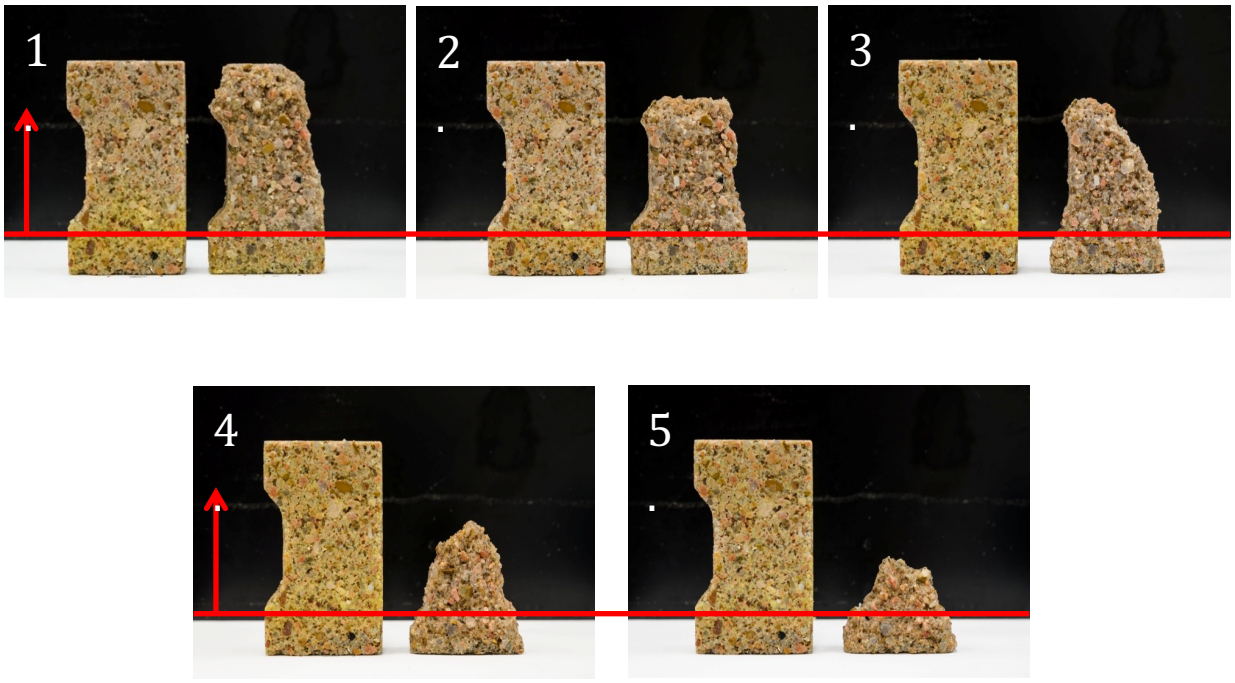

Figure 3. *Time-lapse photos of acid erosion test on Sol-158-3 Masonry treated concrete (left block) and pristine concrete (right block). The red lines and arrows indicate the part of concrete submerged in acid.*

Qualitative Evaluation of Bacterial Growth

Sample 0

As shown in Figure 1, Sample 0 exhibited a high SRB concentration, quantified at approximately 10^5- 10^6 per mL. Visual inspection revealed blackening of the medium and masonry degradation.

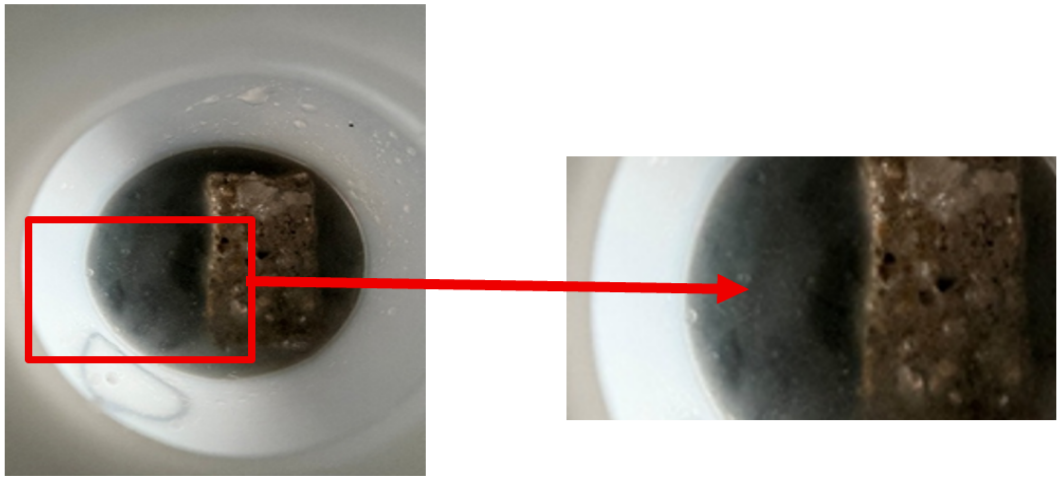

Figure 4. *Microbial Colonization of Unprotected Masonry (Sample 0).*

Sample 0 (control) appears completely black in the test medium, indicating a high SRB concentration (10^5-10^6 per mL). Surface spotting and internal penetration of the concrete matrix are visible, alongside significant masonry degradation and bacterial inundation of dust particles.

Sample A

In contrast to the control (Sample 0), Sample A showed negligible bacterial activity. As illustrated in Figure 2, the test medium remained relatively clear, indicating an SRB concentration of 10^1 – 10^2 per mL.

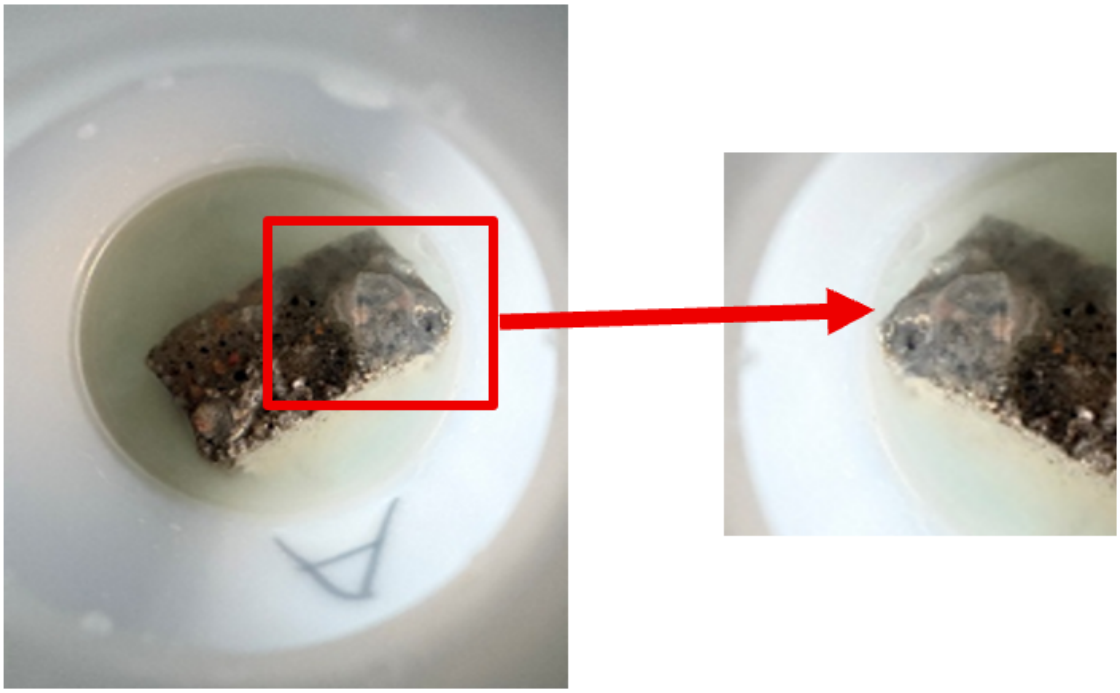

Figure 5. *Microbial Colonization of Masonry Coated in Sol-158-3 (Sample A).*

Sample A

Shows no reaction in the test medium after a 2-minute immersion. This indicates a negligible SRB concentration (10^1–10^2 per mL) and suggests that the Sol-158 coating effectively inhibited bacterial growth compared to Sample 0.

Sample B

Sample B: treated with Sol-158-3 along with an industry standard antibacterial agent, IPBC, exhibited low SRB presence (10^2–10^3 per mL). As seen in Figure 3, while internal penetration was reduced, surface degradation was still observed.

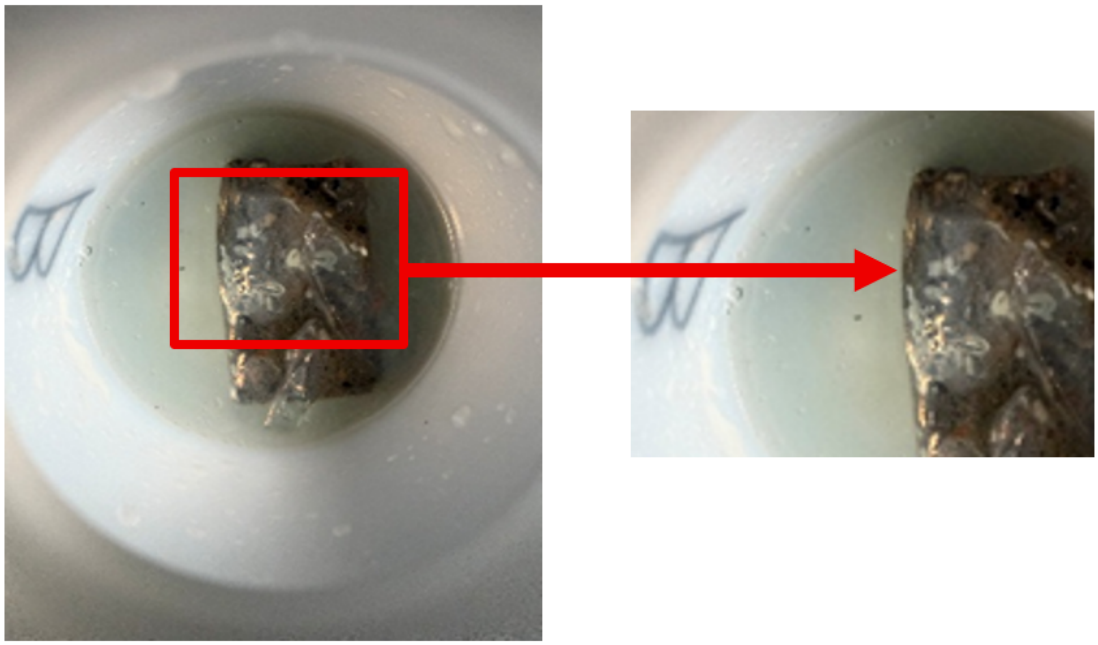

Figure 6. *Microbial Colonization of Masonry with Sol-Gel and Antibacterial Coating (Sample B).*

Sample B: Shows a slight blackening of the medium, indicating low SRB activity (10^2–10^3 per mL). Although the internal coating limited the deep penetration of SRB, the industry-standard antibacterial agent allowed for gradual surface colonization and masonry degradation.

Sample C

Sample C: Represents the industry-standard antibacterial treatment for fracking site masonry, showed moderate SRB presence. As indicated in Figure 4, the test medium developed a narrow black zone, corresponding to an SRB concentration of 10^4–10^5 per mL.

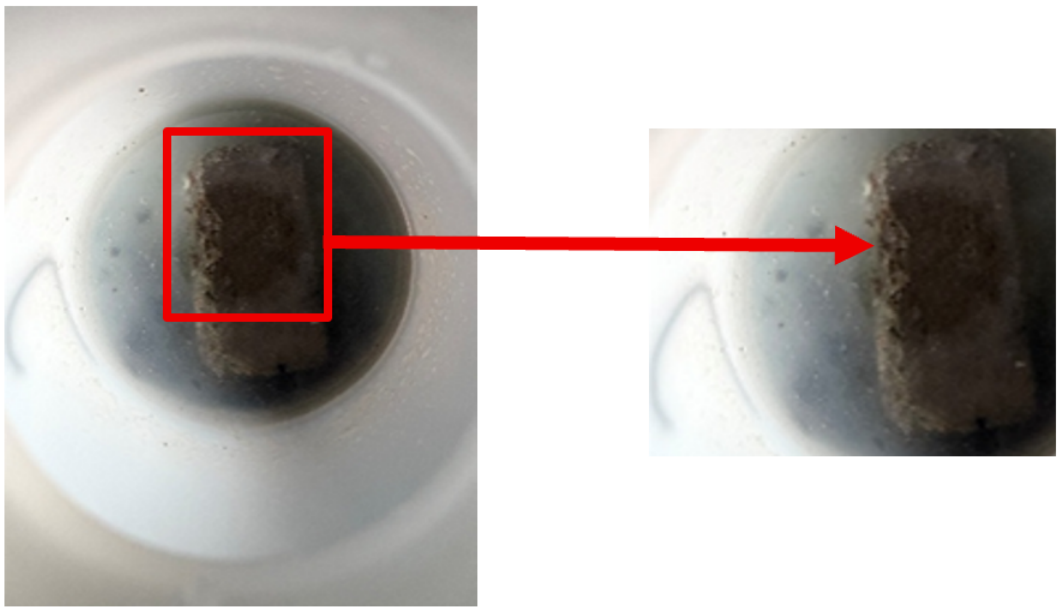

Figure 7. *Microbial Colonization of Masonry Treated with Industry-Standard Antibacterial Agent (Sample C).*

Sample C: Displays a narrow black reaction zone characterized by an SRB presence of 10^4–10^5 per mL. Observations signify surface degradation of the concrete and heavy bacterial presence on adjacent particles, suggesting limited long-term protection compared to experimental treatments.

FTIR Spectroscopic Analysis

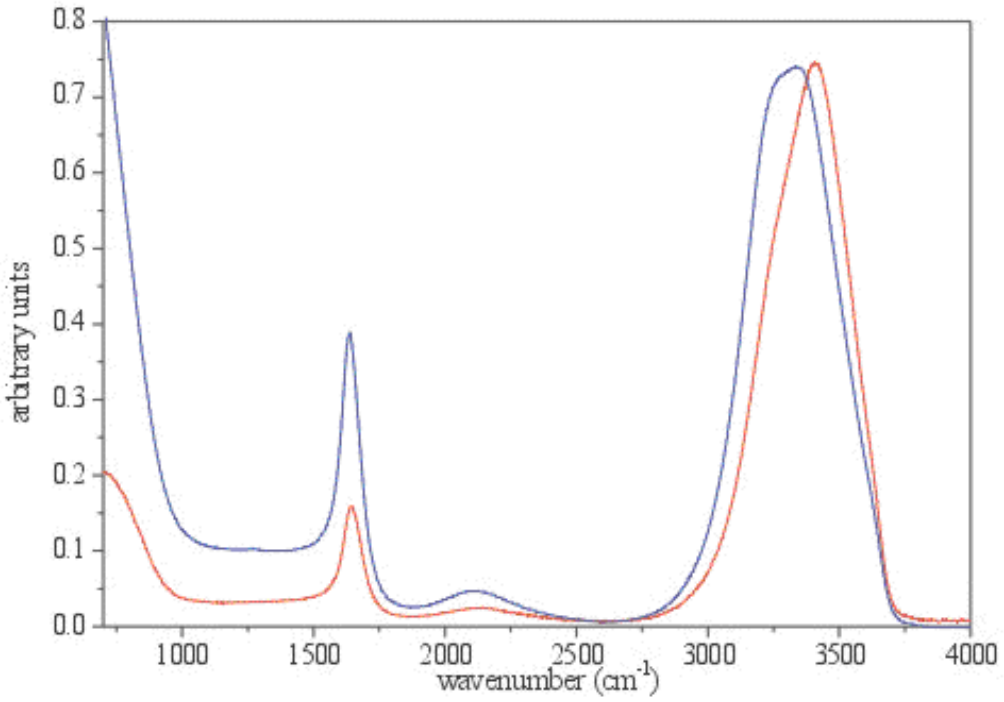

Figure 8. *The spectrum of liquid water recorded with a 2mm thick normal liquid cell with ZnSe windows in transmission mode (red spectrum) and original ATR spectrum (blue spectrum), both normalized to the OH stretching intensity. From "An Attenuated Total Reflection Infrared Spectroscopy of Water Solutions," by J. Grdadolnik, 2002, Int. J. Vib. Spect., 6(2). Copyright © 2026 by Infrared and Raman Discussion Group.*

For a vibration to be detected by FTIR, it must result in a change in the molecule's dipole moment. To accurately track the presence of bacterial cells, their extracellular polymeric substances (EPS), and associated metabolic activity across treated samples, their peak assignments were supported by established biochemical spectral markers. The proliferation of bacteria in the samples and the subsequent degradation of masonry samples is characterized by 6 distinct spectral windows. The lipid region, ranging from 3000 – 2800 cm^{-1}, reflects functional groups like membrane fatty acids and specific amino acid side-chain vibrations. These functional groups are dominated by the asymmetric and symmetric C-H stretching vibrations of CH_3 and CH_2 functional groups. The protein region, between 1800 – 1500 cm^{-1}, contains the definitive Amide I (~1650cm^{1}) and Amide II (~1535cm^{-1}) peaks, serving as strong evidence of protein structure, in addition to

ester functional groups in lipids and nucleic acid transmittance. The mixed zone, spanning from 1500-1200 cm^{-1}, houses proteins, fatty acids, and compounds containing the asymmetric phosphodiester stretching (P=O) of nucleic backbones (found in DNA/RNA) that overlap with Amide III vibrations near 1235 cm^{-1} [34]. The carbohydrate/polysaccharide envelope, between 1200 – 950 cm^{-1}, reflects the complex C-O-C glycosidic link vibrations characteristic of extracellular biofilm matrices [35]. Spectral contributions around 1130 – 1100cm^{-1} are assigned to ionic sulfate (SO_4^{2-}) stretching vibrations, providing a direct metric for evaluating concrete degradation caused by biogenic sulfuric acid [36].

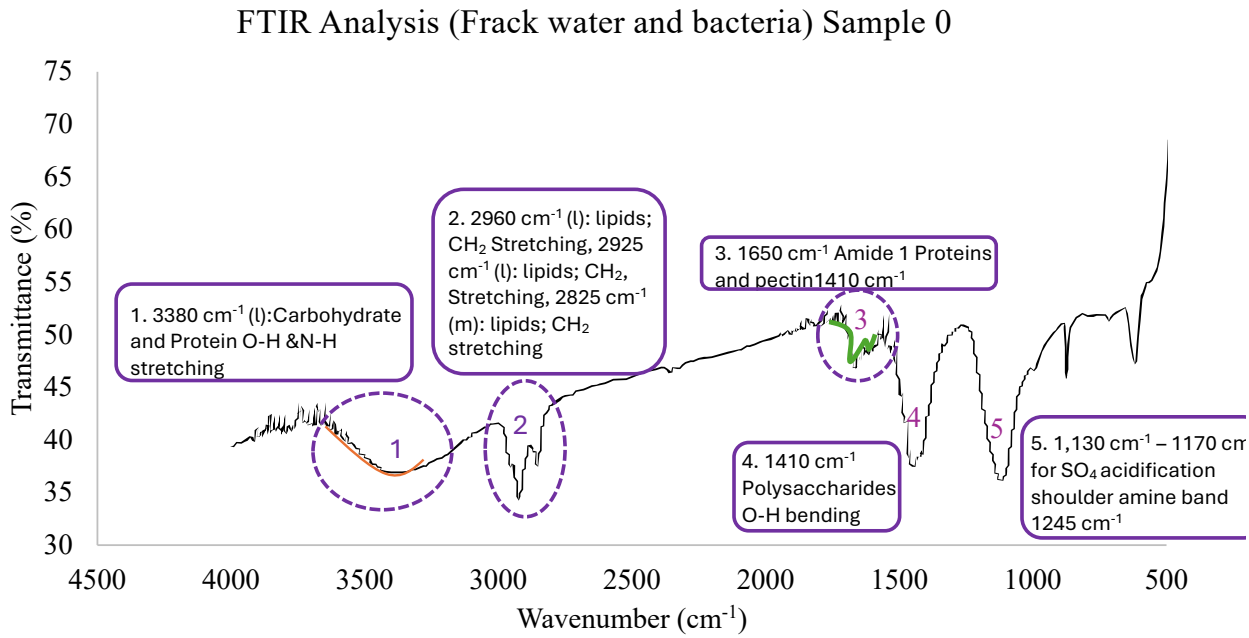

Figure 9. *Shown is the spectrum of masonry and water from sample 0, which is used to gain an insight into the response of frack water with bacteria consuming the masonry present. The C=O stretching of amide (protein) or carboxyl groups, which is suggestive of the lipid and protein components of the cell wall, is responsible for a significant peak at 1622.6 cm-1. Another standout but typically expected is the asymmetric CH3 bending of the methyl groups of lipids at 1430 cm-1. However, the overreaching signals of water dominate, yet the FTIR can still deliver significant value and fingerprinting [37].*

As seen in Fig. 7, two vibrations are expected in the regions between 2800 cm^{-1} and 3600 cm^{-1}, the first one is associated with symmetric stretch, whereas the second one is associated with asymmetric stretch. Vibrational modes at 3280 cm^{-1}, which correspond to O-H or N-H stretching vibrations, suggest changes in the hydrogen bonding environment. This could occur if some of the minerals within the concrete have amine or hydroxyl groups, changing the ways in which they

respond spectroscopically. Beyond this, there is a prominent peak at 2922 cm^{-1} that can represent the C-H stretching of methylene groups. These strong peaks are frequently referred to as C-H stretch in (Lipids) at 2922.2 cm^{-1}, indicating minimal change in the aliphatic chains of lipids or proteins. Significant transmittance changes in the carbohydrate region (1300-1000 cm^{-1}), specifically at 1054.8 cm^{-1} alongside shifting nucleic acid and cell wall markers at 1230cm^{-1}, indicate an abundance of polysaccharides. This structural profile is consistent with a thriving bacterial growth process.

The presence of dissolved organic matter, as evidenced by the peaks at 1635 cm^{-1} are attributed to C=O and COO^- vibrations of carboxylate functional groups and the deformation of CH groups [38]. In aqueous models, this region experiences a strong spectral overlap with the bending and stretching modes of -OH groups [39]. These combined peaks serve as reliable indicators of the natural organic matter present in each sample.

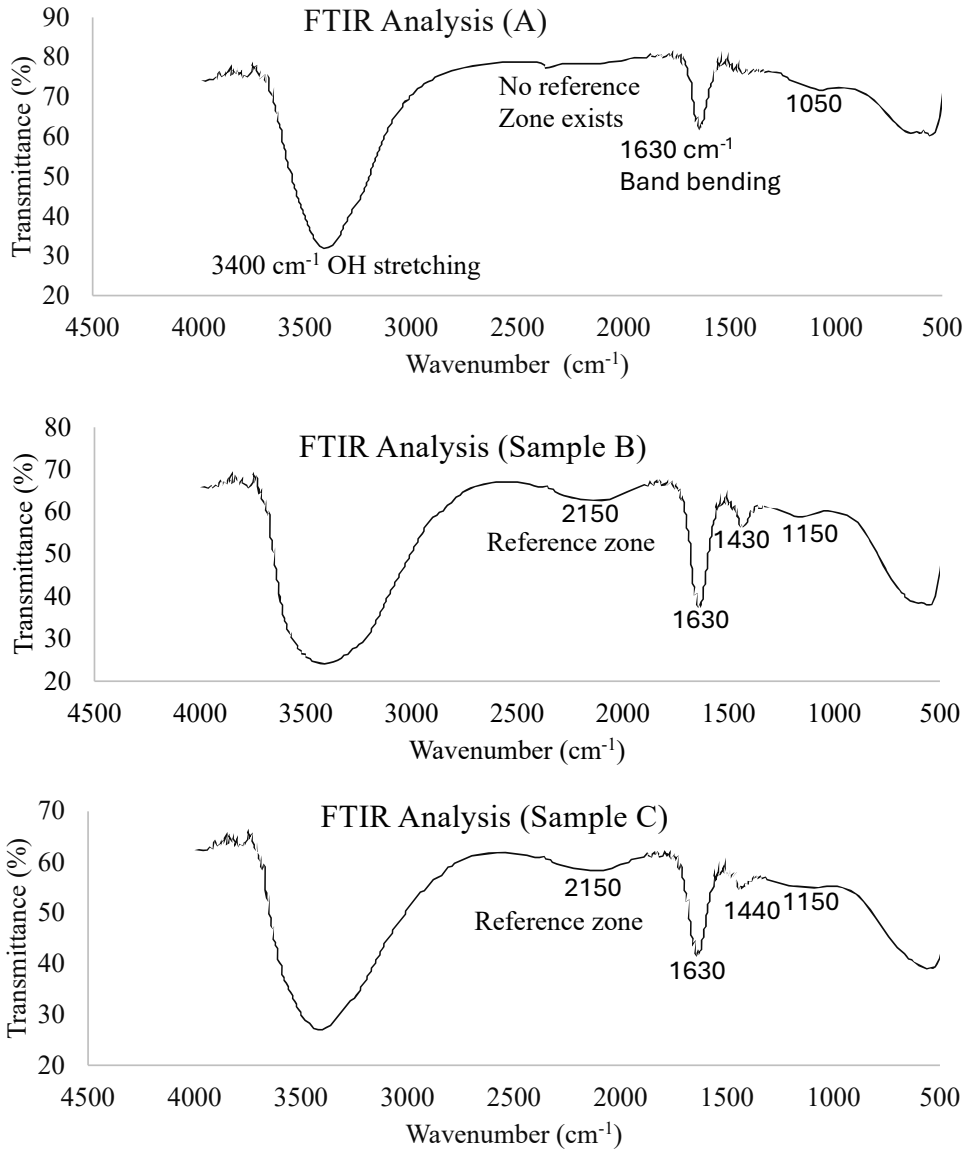

Figure 10. *Fourier-transform infrared (FTIR) spectra analysis comparing functional groups across three distinct samples. Sample A shows no reference zone, whereas Samples B and C exhibit a distinct reference peak at 2150cm⁻¹. Key vibrational bands are annotated, including O-H stretching near 3400cm⁻¹ and bending vibrations at 1630cm⁻¹.*

Polysaccharides are key components in hydraulic fracturing (fracking) fluids, where they act as thickeners and viscosifiers, while bacteria play a complex role in degrading these substances and affecting the resulting wastewater. The introduction of polysaccharides, such as guar gum and cellulose, into deep subsurface environments can promote the growth of specific bacteria, which can then lead to operational issues like biogenic sulfide production. The nutrient for this chemical

interaction, and consequently the growth of bacterial damage, is through this localized chemical interaction, acting as a food source [40,41]. Importantly, while the bacteria's presence is poorly reflected, it can be seen from the polysaccharide mode found at 1450 cm^{-1} and less so at 1440 cm^{-1} [42]. The structural peak at 1150 cm^{-1} remains consistent with localized cellulose formation, reflecting the characteristic C-O-C asymmetrical stretching of the structural polysaccharide backbone [43]. This is a clear indication that for samples B and C, the environment is limited, yet still allows for ultra-slow growth of bacteria, giving rise to further internal sulphate production and the potential of increasing bacteria presence as it erodes the masonry during the growing phases. Sample A is very typical of what was obtained and observed visually, with no real bacterial growth and no sign of the polysaccharides' growth.

Discussion

The superior performance of Sol-158 is fundamentally rooted in its unique interaction with the masonry substrate. Traditional organic coatings, such as epoxies, often suffer from poor adhesion because they sit on the surface of masonry as a separate layer. Contrastingly, the utilization of an alcohol-based solvent in Sol-158-3 allows for miscible displacement, where the alcohol mixes with and replaces the water trapped within the masonry pores. This process, catalyzed by 0.1M of HCl, ensures that Sol-158-3 penetrates deep into the pore structure, facilitating the formation of bonds with the masonry matrix. This creates a masonry jacket that is chemically integrated as opposed to a separate layer, effectively eliminating the risk of delamination. Additionally, by inhibiting the initial colonization of neutrophilic sulfur-oxidizing bacteria, the coating prevents the chemical interaction that drops the surface pH. Maintaining this higher pH environment effectively inhibits aggressive acidophilic sulfur-oxidizing bacteria that thrive in extreme acidity [18].

More importantly, when tracking the samples exposed to bacteria, the FTIR spectra of Samples B and C reveal sharp carbohydrate-associated peaks at 1450cm^{-1} and 1440cm^{-1}, indicating

significant polysaccharide deposition from active bacterial biofilms. In contrast, Sample A shows a nearly total suppression of these polysaccharide vibrational modes. This demonstrates molecular-level evidence that Sol-158-3 actively prevents bacteria from establishing a matrix upon the concrete sample.

While traditional nanocomposite coatings often fail due to nanoparticle agglomeration, Sol-158-3's ability to form a nanoporous network provides a uniform barrier where bacteria are unable to establish a stable biofilm. This effectively inhibits the biogenic production of sulfuric acid at the source. Moreover, this prevents the chemical decomposition of the cement, which avoids the formation of gypsum and ettringite, which are often responsible for mechanical deterioration in masonry [44]. This prevention is validated by the mass retention and acid erosion results. While the pristine concrete sample underwent significant surface dissolution and massive weight loss under acid testing, Sol-158-3 treated samples maintained a near-perfect mass retention. This high mass retention under extreme acidic conditions proves that Sol-158-3 can endure harsh environments created by active sulfate reduction and oxidation without degrading.

Interestingly, the experimental results indicated that pure Sol-158-3 coating exhibited superior mitigation of SRB presence compared to the Sol-158-3 and IPBC admixture. This may be attributed to the steric hindrance caused by the bulky IPBC molecules, which likely disrupted cross-linking during polycondensation [45]. When IPBC is added after the application of Sol-158-3, it disturbs the coating's ability to effectively protect the masonry sample by exceeding the critical concentration threshold of the admixture coating, potentially increasing the permeability of the masonry jacket. Furthermore, pure Sol-158-3 likely achieved a more uniform, hydrophobic surface, which proved more effective at physically preventing microbial attachment, as opposed to the chemically active additive IPBC. This mechanism is further explained by the mass retention kinetics coupled with the FTIR analysis of samples treated with IPBC. The severe wight loss and

structural degradation observed in samples treated with Pristine directly highlight the limitations of standard barrier formations when subjected to extreme acid attacks. Conversely, the exceptionally high mass retention of samples treated with Sol-158-3 confirms the superior resilience of the sol-gel network. By blocking the physical penetration of acids and inhibiting the anchoring of bacteria, Sol-158-3 achieves an optimal shielding effect. This suggests that for MIC mitigation, the structural integrity and density of Sol-158-3's barrier is more crucial than the utilization of organic biocides. This is an important step towards environmentally favorable solutions, as reducing the use of organic biocides like IPBC could eliminate leaching that poses significant environmental risks to local ecosystems.

Figure 11. Heavily degraded by water damage, corroded pipes stand near a pier in the factory area of the abandoned limestone quarry on Furilden, Gotland, Sweden. Source: Wikipedia Commons

Sol-158-3's protective characteristics signify a shift towards proactive infrastructure protection. The findings of this study have significant implications for the management of industrial infrastructure and deeply embedded pipelines. By demonstrating that pure Sol-158-3 is more effective at MIC mitigation without the need for additives, this research offers a cost-effective, sustainable pathway for masonry protection. Given the $2.5 trillion global annual cost of corrosion, transitioning to proactive masonry shielding has the potential to drastically extend the service life of masonry infrastructure.

While this study established the efficacy of the sol-gel barrier against SRB, future work should investigate the long-term durability of the coating under conditions that mirror truly harsh environments. Moreover, field-scale testing in active embedded pipeline environments is recommended to validate the lab-scale findings against the complex biofilms found in real-world infrastructure.

Conclusion

This study evaluates the capability of Sol-158-3 to effectively inhibit the presence of SRB, the primary drivers of MIC. The experimental data reveal that pure Sol-158-3 provides an effective antimicrobial barrier that starves SRB by restricting the capillary entry of sulfate-rich water. Additionally, the inclusion of organic biocides like IPBC can interfere with the coating's structural density, reducing its overall efficacy. By preventing the initial pH drop driven by neutrophilic bacteria, the coating successfully inhibits the transition to highly aggressive sulfate-oxidizing stages. Ultimately, this approach to antimicrobial protection offers a durable, environmentally friendly, and industrially scalable strategy for preserving the world's concrete and masonry infrastructure. The results suggest a significant innovation that could substantially extend the lifespan of masonry infrastructure. Furthermore, the removal of chemical biocides like IPBC offers

an eco-friendly approach to surface protection, eliminating the environmental toxicity associated with traditional chemical treatments while reducing material costs.

References

[1] World Corrosion Organization. Corrosion Awareness Day, 24th April. **2024**. https://corrosion.org/Events/Corrosion+Awareness+Day/2024_+April+24-p-2706.html

[2] Shaw, B. A.; Kelly, R. G. What Is Corrosion? *Electrochemical Society Interface* **2006**, *15* (1). https://doi.org/10.1149/2.f06061if

[3] Koch, G.; Varney, J.; Thompson, N.; Moghissi, O.; Gould, M.; Payer, J. International Measures of Prevention, Application, and Economics of Corrosion Technologies Study. *Challenges in Corrosion* **2016**.

[4] Skovhus, T. L.; Enning, D.; Lee, J. S. *Microbiologically Influenced Corrosion in the Upstream Oil and Gas Industry*. **2017**. https://doi.org/10.1201/9781315157818

[5] Noeiaghaei, T.; Mukherjee, A.; Dhami, N.; Chae, S. R. Biogenic Deterioration of Concrete and Its Mitigation Technologies. *Construction and Building Materials* **2017**, *149*. https://doi.org/10.1016/j.conbuildmat.2017.05.144

[6] Dunuweera, S. P.; Rajapakse, R. M. G. Cement Types, Composition, Uses and Advantages of Nanocement, Environmental Impact on Cement Production, and Possible Solutions. *Advances in Materials Science and Engineering* **2018**. https://doi.org/10.1155/2018/4158682

[7] Zivica, V.; Bajza, A. Acidic Attack of Cement Based Materials—A Review. Part 1. Principle of Acidic Attack. *Construction and Building Materials* **2001**, *15* (8). https://doi.org/10.1016/S0950-0618(01)00012-5

[8] Wang, Y.; Wen, S.; Zhang, S.; Tang, Y.; Yuan, X.; Guan, F.; Duan, J. Unraveling the Source of Corrosive Microorganisms from Fracturing Water to Flowback Water in Shale Gas Field: Evidence from Gene Sequencing and Corrosion Tests. *Frontiers in Microbiology* **2025**, *16*. https://doi.org/10.3389/fmicb.2025.1552006

[9] Deng, X.; Dohmae, N.; Nealson, K. H.; Hashimoto, K.; Okamoto, A. Multi-Heme Cytochromes Provide a Pathway for Survival in Energy-Limited Environments. *Science Advances* **2018**, *4* (2). https://doi.org/10.1126/sciadv.aao5682

[10] Tripathi, A. K.; Thakur, P.; Saxena, P.; Rauniyar, S.; Gopalakrishnan, V.; Singh, R. N.; Gadhamshetty, V.; Gnimpieba, E. Z.; Jasthi, B. K.; Sani, R. K. Gene Sets and Mechanisms of Sulfate-Reducing Bacteria Biofilm Formation and Quorum Sensing With

Impact on Corrosion. *Frontiers in Microbiology* **2021**, *12*, 754140. https://doi.org/10.3389/fmicb.2021.754140

[11] Stott, J. F. D. Corrosion in Microbial Environments. In *Shreir's Corrosion*; Elsevier: Oxford, **2010**; pp 1169–1190.

[12] Marciales, A.; Peralta, Y.; Haile, T.; Crosby, T.; Wolodko, J. Mechanistic Microbiologically Influenced Corrosion Modeling—A Review. *Corrosion Science* **2019**, *146*. https://doi.org/10.1016/j.corsci.2018.10.004

[13] Joseph, A. P.; Keller, J.; Bustamante, H.; Bond, P. L. Surface Neutralization and H_2S Oxidation at Early Stages of Sewer Corrosion: Influence of Temperature, Relative Humidity and H_2S Concentration. *Water Research* **2012**, *46* (13). https://doi.org/10.1016/j.watres.2012.05.011

[14] Chaudhari, B.; Panda, B.; Šavija, B.; Paul, S. C. Microbiologically Induced Concrete Corrosion: A Concise Review of Assessment Methods, Effects, and Corrosion-Resistant Coating Materials. *Materials* **2022**, *15* (12), 4279. https://doi.org/10.3390/ma15124279

[15] Enning, D.; Garrelfs, J. Corrosion of Iron by Sulfate-Reducing Bacteria: New Views of an Old Problem. *Applied and Environmental Microbiology* **2014**, *80* (4). https://doi.org/10.1128/AEM.02848-13

[16] Kuhl, M.; Jorgensen, B. B. Microsensor Measurements of Sulfate Reduction and Sulfide Oxidation in Compact Microbial Communities of Aerobic Biofilms. *Applied and Environmental Microbiology* **1992**, *58* (4). https://doi.org/10.1128/aem.58.4.1164-1174.1992

[17] Lin, J. Y.; Wang, G. J.; Lee, J. Y.; Wu, Y. L.; Wang, C. Y. Selective Oxidation of H_2S to Elemental Sulfur over Waste PEevaT-Derived Biochar-Supported Metal Catalysts. *ACS Omega* **2025**, *10* (50). https://doi.org/10.1021/acsomega.5c08359

[18] Pramanik, S. K.; Bhuiyan, M.; Robert, D.; Roychand, R.; Gao, L.; Cole, I.; Pramanik, B. K. Bio-Corrosion in Concrete Sewer Systems: Mechanisms and Mitigation Strategies. *Science of the Total Environment* **2024**, *921*, 171231. https://doi.org/10.1016/j.scitotenv.2024.171231

[19] Rooyackers, F. A. M.; Bosco, E.; Suiker, A. S. J.; Clemens, F. H. L. R. A Chemo-Mechanical Model for Biogenic Sulphide Corrosion of Concrete. *Cement and Concrete Research* **2022**, *160*. https://doi.org/10.1016/j.cemconres.2022.106809

[20] U.S. Energy Information Administration. Number of Natural Gas and Oil Wells Drilled. n.d. https://www.eia.gov/dnav/ng/ng_enr_drill_s1_m.htm

[21] Gao, C. H. Drilling Fluids for Shale Fields: Case Studies and Lessons Learnt. *Unconventional Resources* **2024**, *4*. https://doi.org/10.1016/j.uncres.2023.100070

[22] Syed, T. Pre & Post Well Integrity Methods for Hydraulically Fractured/Stimulated Wells. EPA Hydraulic Fracturing Workshop, Arlington, VA, **2011**. https://19january2021snapshot.epa.gov/sites/static/files/documents/pre_post_well_integrity_methods_for_hydraulically_fractured_stimulated_wells.pdf

[23] Jackson, R. B.; Lowry, E. R.; Pickle, A.; Kang, M.; DiGiulio, D.; Zhao, K. The Depths of Hydraulic Fracturing and Accompanying Water Use Across the United States. *Environmental Science and Technology* **2015**, *49* (15). https://doi.org/10.1021/acs.est.5b01228

[24] Liu, J.-F.; Zhang, X.-Y.; Yu, L.-Y.; Wang, X.-L.; Lu, Y.-H.; Zhang, Z.-H.; Jian, Z.-J. Casing Damage in Oil and Water Wells: Causes and Prevention. *Deep Resources Engineering* **2025**. https://doi.org/10.1016/j.deepre.2025.100200

[25] Thi Xuan Hang, T.; Truc, T. A.; Nam, T. H.; Oanh, V. K.; Jorcin, J. B.; Pébère, N. Corrosion Protection of Carbon Steel by an Epoxy Resin Containing Organically Modified Clay. *Surface and Coatings Technology* **2007**, *201* (16–17). https://doi.org/10.1016/j.surfcoat.2007.02.009

[26] Wang, X.; Li, W.; Wang, X.; Bu, M.; Sun, X.; Zhao, Z.; Xu, L.; Chen, L.; Li, Z.; Tebyetekerwa, M. Improved Properties of Epoxy Composite Coatings Enabled by Multi-Dimension Filler Materials. *Progress in Organic Coatings* **2024**, *197*, 108800. https://doi.org/10.1016/j.porgcoat.2024.108800

[27] Ghanbari, A.; Attar, M. M. A Study on the Anticorrosion Performance of Epoxy Nanocomposite Coatings Containing Epoxy-Silane Treated Nano-Silica on Mild Steel Substrate. *Journal of Industrial and Engineering Chemistry* **2015**, *23*. https://doi.org/10.1016/j.jiec.2014.08.008

[28] Chopra, I.; Ola, S. K.; Priyanka; Dhayal, V.; Shekhawat, D. S. Recent Advances in Epoxy Coatings for Corrosion Protection of Steel: Experimental and Modelling Approach—A Review. *Materials Today: Proceedings* **2022**, *62*. https://doi.org/10.1016/j.matpr.2022.04.659

[29] Faleye, O. O.; Faleye, O. S.; Lee, J. H.; Lee, J. Antibacterial and Antibiofilm Activities of Iodinated Hydrocarbons against Vibrio parahaemolyticus and Staphylococcus aureus. *Scientific Reports* **2024**, *14* (1). https://doi.org/10.1038/s41598-024-55479-7

[30] McNeely, B. 2 Ways to Prevent Microbial-Induced Corrosion. Gainy's. **2025**. https://www.gaineysconcrete.com/post/2-ways-to-prevent-microbial-induced-corrosion

[31] Qiu, L.; Dong, S.; Ashour, A.; Han, B. Antimicrobial Concrete for Smart and Durable Infrastructures: A Review. *Construction and Building Materials* **2020**, *260*, 120456. https://doi.org/10.1016/j.conbuildmat.2020.120456

[32] Haile, T.; Nakhla, G.; Allouche, E.; Vaidya, S. Evaluation of the Bactericidal Characteristics of Nano-Copper Oxide or Functionalized Zeolite Coating for Bio-Corrosion Control in

Concrete Sewer Pipes. *Corrosion Science* **2010**, *52* (1). https://doi.org/10.1016/j.corsci.2009.08.046

[33] Wang, A. J.; Maharjan, S.; Liao, K. S.; McElhenny, B. P.; Wright, K. D.; Dillon, E. P.; Neupane, R.; Zhu, Z.; Chen, S.; Barron, A. R.; Varghese, O. K.; Bao, J.; Curran, S. A. Poly(octadecyl acrylate)-Grafted Multiwalled Carbon Nanotube Composites for Wearable Temperature Sensors. *ACS Applied Nano Materials* **2020**, *3* (3). https://doi.org/10.1021/acsanm.9b02396

[34] Tiquia-Arashiro, S.; Li, X.; Pokhrel, K.; Kassem, A.; Abbas, L.; Coutinho, O.; Kasperek, D.; Najaf, H.; Opara, S. Applications of Fourier Transform-Infrared Spectroscopy in Microbial Cell Biology and Environmental Microbiology: Advances, Challenges, and Future Perspectives. *Frontiers in Microbiology* **2023**, *14*. https://doi.org/10.3389/fmicb.2023.1304081

[35] Kamnev, A. A.; Dyatlova, Y. A.; Kenzhegulov, O. A.; Fedonenko, Y. P.; Evstigneeva, S. S.; Tugarova, A. V. Fourier Transform Infrared (FTIR) Spectroscopic Study of Biofilms Formed by the Rhizobacterium Azospirillum baldaniorum Sp245: Aspects of Methodology and Matrix Composition. *Molecules* **2023**, *28* (4). https://doi.org/10.3390/molecules28041949

[36] Nasrazadani, S.; Eghtesad, R.; Sudoi, E. et al. Application of Fourier transform infrared spectroscopy to study concrete degradation induced by biogenic sulfuric acid. *Mater Struct* **2016**, *49*, 2025–2034.

[37] Abdulelah, H.; Mahmood, S. M.; Al-Hajri, S.; Hakimi, M. H.; Padmanabhan, E. Retention of Hydraulic Fracturing Water in Shale: The Influence of Anionic Surfactant. *Energies* **2018**, *11* (12). https://doi.org/10.3390/en11123342

[38] Duan, J.; Sontarp, E. J.; Myneni, S. C. B. Detecting Structural Environments of Carboxyl Groups in Dissolved Natural Organic Molecules. *ACS ES&T Water* **2024**, *4* (2). https://doi.org/10.1021/acsestwater.3c00609

[39] Max, J. J.; Chapados, C. Infrared Spectroscopy of Aqueous Carboxylic Acids: Comparison between Different Acids and Their Salts. *Journal of Physical Chemistry A* **2004**, *108* (16). https://doi.org/10.1021/jp036401t

[40] Cliffe, L.; Hernandez-Becerra, N.; Boothman, C.; Eden, B.; Lloyd, J. R.; Nixon, S. L. Guar Gum Stimulates Biogenic Sulfide Production in Microbial Communities Derived from UK Fractured Shale Production Fluids. *Microbiology Spectrum* **2022**, *10* (6). https://doi.org/10.1128/spectrum.03640-22

[41] Nixon, S. L.; Walker, L.; Streets, M. D. T.; Eden, B.; Boothman, C.; Taylor, K. G.; Lloyd, J. R. Guar Gum Stimulates Biogenic Sulfide Production at Elevated Pressures: Implications for Shale Gas Extraction. *Frontiers in Microbiology* **2017**, *8*. https://doi.org/10.3389/fmicb.2017.00679

[42] Leppänen, I.; Vikman, M.; Harlin, A.; Orelma, H. Enzymatic Degradation and Pilot-Scale Composting of Cellulose-Based Films with Different Chemical Structures. *Journal of Polymers and the Environment* **2020**, *28* (2). https://doi.org/10.1007/s10924-019-01621-w

[43] Marelli, F.; Pontoriero, D.; Antonini, C.; Tagliaro, I. Water-Polysaccharide Interactions and Their Properties in Freezing Conditions. *Carbohydrate Polymers* **2025**, *368*, 124138. https://doi.org/10.1016/j.carbpol.2025.124138

[44] Godinho, J. P.; Medeiros, M. H. F.; Melo Neto, A. A.; Lima, V. M. E.; de Souza, D. J. Laboratory–Field Assessment of Concrete Exposed to Biogenic Sulphuric Acid: Influence of SCM-Based Binders on Long-Term Degradation. *Construction and Building Materials* **2025**, *493*, 143185. https://doi.org/10.1016/j.conbuildmat.2025.143185

[45] Bera, S.; Rout, T. K.; Udayabhanu, G.; Narayan, R. Comparative Study of Corrosion Protection of Sol-Gel Coatings with Different Organic Functionality on Al-2024 Substrate. *Progress in Organic Coatings* **2015**, *88*. https://doi.org/10.1016/j.porgcoat.2015.07.006